Arch Appl Mech
https://doi.org/10.1007/s00419-019-01590-5

**Malla Reddy Perati · Sindhuja Ala · Rajitha Gurijala**

# Study of reflection and transmission of axially symmetric body waves incident on a base of semi-infinite poroelastic solid cylinder

Received: 12 April 2019 / Accepted: 26 August 2019


**Abstract** This paper deals with the study of the reflection and transmission phenomena when axial symmetric body waves incident on the base of a poroelastic semi-infinite solid cylinder, surrounded by another medium. Cylinder is assumed to be isotropic so that Biot's theory of poroelasticity can be employed. Reflection and transmission coefficients are computed as a function of angle of incidence in the case of permeable base. In addition, square root of energy ratio is computed for the body waves. Numerical results are presented graphically for two types of poroelastic solids, namely sandstone saturated with kerosene and sandstone saturated with water.

**Keywords** Poroelastic solid cylinder · Reflection · Transmission · Energy ratio · Angle of incidence

## 1 Introduction

The wave reflection and transmission phenomena have long history and received much attention during the past half-century in many scientific fields, such as Marine Seismology, Geotechnical Engineering, Acoustics and Geophysics. Analysis of reflection and transmission phenomena can be used to understand the various materials. Sandstone is a great source for quartz which is very useful in day-to-day life. Sandstone deposits are cylindrical in shape and surrounded by poroelastic medium soil or rock. The study of reflection and transmission of waves incidented at the interface gives the information pertaining to sandstone deposits. The reflection and transmission coefficients are generally based on the medium consisting of two non-homogeneous layers separated by a horizontal interface. In Acoustics, the said coefficients are used to understand the effect of various materials on their acoustic environments. In the research domains such as Geophysics and Medicine, the pertinent analysis can be used as nondestructive evaluation (NDE) tool. Displacement discontinuities conserve energy and yield frequency-dependent reflection and transmission coefficients. To the best of author's knowledge, some of the contributions in this domain are as follows. Reflection and transmission coefficients for harmonic plane waves incident at arbitrary angles upon a plane linear slip interface are computed in the case of elastic media [1]. Employing transfer matrix method, Bogy and Gracewski [2] derived the plane wave reflection coefficient for a layered solid half-space. In the paper [2], the reflection coefficient is derived for an isotropic, homogeneous elastic layer of arbitrary thickness that is perfectly bonded to such an elastic half-space when plane waves are incident from an inviscid fluid onto the layered solid. Singh [3] discussed the reflection of $P$- and $SV$-waves from the free surface of an elastic solid with generalized thermo-diffusion. In the paper [3], it is concluded that the reflection coefficients depend upon the angle of incidence of P- and SV-waves and thermo-diffusion parameters. Amplitude ratios and energy ratios are computed numerically, and the conservation of energy across the interface is verified for an elastic solid half-space [4]. Kumar et al.

M. R. Perati · S. Ala · R. Gurijala (✉)
Department of Mathematics, Kakatiya University, Warangal, Telangana, India
E-mail: rajitha.akshu@gmail.com

Published online: 20 September 2019

[5] investigated the reflection and transmission of plane waves at the loosely bonded interface of an elastic solid half-space and a micropolar thermo-elastic diffusion half-space. In the paper [5], the effects of relaxation times and loosely bonding parameters shown in energy ratios for a specific model. The analytical expressions for amplitude ratios, reflection and transmission coefficients in terms of angles and material parameters have been obtained for quasi-longitudinal and quasi-transverse wave incidence [6]. Reflection and transmission of elastic waves from the boundary of a fluid-saturated porous solid are discussed by Wu et al. [7]. Santos et al. [8] showed the importance of inclusion of the frequency correction factor to analyze wave propagation for frequency varying between the seismic and ultrasonic ranges. Propagator matrix method is applied for calculation of reflected coefficients in the case of inhomogeneous, anisotropic, poroelastic seafloor [9]. In the paper [9], the matrix is integrated using an implicit technique. For generalized thermo-elastic medium, the reflection phenomena of SV-waves are discussed by Abd-Alla and Al-Dawy [10]. In the paper [10], the reflection coefficient is calculated for shear wave that incident from within the solid on its boundary. Lin et al. [11] studied the reflection of plane waves in a poroelastic half-space saturated with inviscid fluid. The said paper reports the amount of solid frame stiffness controls the response of a fluid-saturated porous system. Employing Biot's theory of poroelasticity [12], the reflection of plane waves at boundaries of a poroelastic half-space is investigated by Tajuddin and Hussaini [13]. In the paper [13], it is clear that the overlapping parameter between solid and fluid plays a significant role in generating the reflected slow dilatational wave. By taking the sealed pore and the open pore boundaries, wave reflection and transmission are discussed in [14]. The said paper revealed that the amplitudes of the reflected and transmitted waves strongly depend on boundary conditions. Novel expressions for the reflection and transmission coefficients in terms of the spectral properties of the governing differential system are given in [15]. Cui and Wang [16] studied reflection and transmission of plane waves at an ocean floor interface. The results of this paper [16] indicate that the effect of the squirt flow is noticeable in the reflection and refraction phenomena. Semi-relativistic reflection and transmission coefficients for two spinless particles separated by exponential and rectangular-shaped potential barriers are investigated by Ethyl et al. [17]. The reflection and transmission of plane waves between two different fluids saturated with porous half-spaces are given in [18]. In the paper [18], the variations of amplitude ratios with angle of incidence are calculated. Corredor et al. [19] investigated scattering problem at all angles of incidence for a single layer embedded between two half-spaces with dissimilar media. Most of the works in this domain are confined to half-spaces. However, to the best of author's knowledge, study of reflection and transmission coefficients is not made extensively in the case of poroelastic cylindrical solids. The propagation of thick-walled hollow poroelastic cylinder under plane strain conditions is studied by Reddy and Tajuddin [20]. The said paper describes transitions from the case of plate to thin shell, and to thick-walled hollow cylinder, and then to solid cylinder. Investigation of reflection and transmission of acoustic waves of a porous solid is made using experimental reflected and transmitted signals [21]. Motivated from the results of said papers, reflection and transmission phenomena are analyzed in the case of a poroelastic solid cylinder. In the present work, reflection, transmission coefficients and energy ratio are computed for the fast $P$-wave $(P-I)$, the slow $P$-wave $(P-II)$ and the shear $(SV)$-wave in the case of permeable base.

This paper is organized as follows. In Sect. 2, formulation and solution of the problem are given. Boundary conditions are given in Sect. 3. In Sect. 4, numerical results are described. Finally, conclusion is given in Sect. 5.

## 2 Formulation and solution of the problem

Consider an isotropic poroelastic solid cylinder whose axis is along $z$-axis of cylindrical coordinate system, surrounded by another medium. Assume axial symmetric body waves that incident at $z = 0$ plane. Because of medium change, two phenomena reflection and transmission do occur. The geometry of the problem is given in Fig. 1. The equations of motion of a homogeneous, isotropic poroelastic solid in absence of dissipation are [12]:

$$\begin{aligned} N\nabla^2\vec{u} + \nabla(Ae + Q\varepsilon) &= \frac{\partial^2}{\partial t^2}(\rho_{11}\vec{u} + \rho_{12}\vec{U}), \\ \nabla(Qe + R\varepsilon) &= \frac{\partial^2}{\partial t^2}(\rho_{12}\vec{u} + \rho_{22}\vec{U}). \end{aligned} \tag{1}$$

where $\vec{u} = (u, v, w)$ and $\vec{U} = (U, V, W)$ are the displacement vectors of solid and fluid, respectively, $e$ and $\varepsilon$ are the dilatations of solid and fluid, and $P = A + 2N$, $Q$ and $R$ are all poroelastic constants. The mass coefficients $\rho_{11}$, $\rho_{12}$ and $\rho_{22}$ satisfy the relations $\rho_1 = \rho_{11} + \rho_{12} = (1-\beta)\rho_s$, $\rho_2 = \rho_{12} + \rho_{22} = \beta\rho_f$,

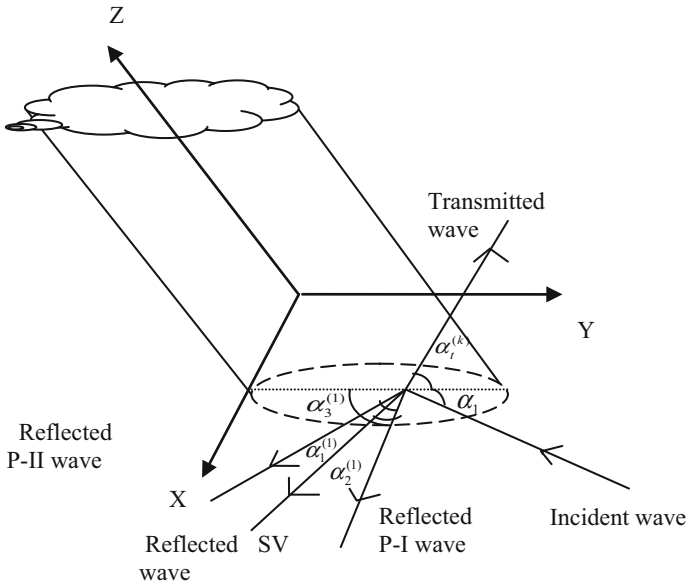


**Fig. 1** Geometry of the problem

$\rho = \rho_1 + \rho_2 = \rho_s + \beta(\rho_f - \rho_s)$ [13]. Here, $\rho_1$ and $\rho_2$ are mass of solid and fluid per unit volume of aggregate, $\rho$ is the total mass of solid–fluid aggregate per unit volume, $\rho_{11}$, $\rho_{12}$ and $\rho_{22}$ are the mass coefficients, $\rho_s$ and $\rho_f$ are the mass density of the solid and fluid, and $\beta$ is the porosity of the aggregate. The solid stresses $\sigma_{ij}$ and fluid pressure $s$ are given by [12]

$$\sigma_{ij} = 2Ne_{ij} + (Ae + Q\varepsilon)\delta_{ij}, \quad (i, j = 1, 2, 3), \quad s = Qe + R\varepsilon. \tag{2}$$

In Eq. (2), $\delta_{ij}$ is the well-known Kronecker delta function.

Consider the following potential decomposition of displacements in the case of axial symmetric waves

$$\begin{aligned} u &= \frac{\partial \phi_1}{\partial r} - \frac{\partial \psi_1}{\partial z}, \quad U = \frac{\partial \phi_2}{\partial r} - \frac{\partial \psi_2}{\partial z}, \\ w &= \frac{\partial \phi_1}{\partial z} + \frac{\partial \psi_1}{\partial r} + \frac{\psi_1}{r}, W = \frac{\partial \phi_2}{\partial z} + \frac{\partial \psi_2}{\partial r} + \frac{\psi_2}{r}. \end{aligned} \tag{3}$$

The displacement potentials $\phi$'s and $\psi$'s functions of $r$, $z$ and $t$ are assumed as given below.

$$\begin{aligned} \phi_1 &= \begin{cases} \phi_{(k)} + \phi_l^{(k)} = A_k e^{i(\omega t - \delta_k (r \sin\alpha_k - z\cos\alpha_k))} + A_l^{(k)} e^{i(\omega t - \delta_l (r \sin\alpha_l^{(k)} - z\cos\alpha_l^{(k)}))}, l, k = 1, 2, \\ \phi_{(3)} + \phi_l^{(k)} = A_k e^{i(\omega t - \delta_k (r \cos\alpha_k - z\sin\alpha_k))} + A_l^{(k)} e^{i(\omega t - \delta_l (r \sin\alpha_l^{(k)} - z\cos\alpha_l^{(k)}))}, \ l, k = 3, \end{cases} \\ \phi_2 &= \begin{cases} \phi_{(k)} + \phi_l^{(k)} = A_k e^{i(\omega t - \delta_k \mu_k (r \sin\alpha_k - z\cos\alpha_k))} + A_l^{(k)} e^{i(\omega t - \delta_l \mu_l (r \sin\alpha_l^{(k)} - z\cos\alpha_l^{(k)}))}, l, k = 1, 2, \\ \phi_{(3)} + \phi_l^{(k)} = A_k e^{i(\omega t - \delta_k \mu_k (r \cos\alpha_k - z\sin\alpha_k))} + A_l^{(k)} e^{i(\omega t - \delta_l \mu_l (r \sin\alpha_l^{(k)} - z\cos\alpha_l^{(k)}))}, \ l, k = 3, \end{cases} \\ \psi_1 &= A_3^{(k)} e^{i(\omega t - \delta_3 (r \sin\alpha_3^{(k)} - z\cos\alpha_3^{(k)}))}, \quad \psi_2 = A_3^{(k)} e^{i(\omega t - \delta_3 \mu_3 (r \sin\alpha_3^{(k)} - z\cos\alpha_3^{(k)}))}. \end{aligned} \tag{4}$$

In the above, $\alpha_k$ is the angle made by the $k$th incident wave with the normal, $\alpha_l^{(k)}$—angle made by the $l$th reflected wave with the normal when $k$th wave is incident, $\phi_{(k)}$—incident wave potential, $\phi_l^{(k)}$—reflected wave potential, $\omega$—frequency, $\delta_k$—wavenumber of incident wave, $\delta_l$—wavenumber of reflected wave, and $Z_l^{(k)} = (A_l^{(k)}/A_k)$—reflection coefficient of $l$th reflected wave when $k$th wave is incident. Using Eq. (4) in (3), after a long calculation, the following solid displacements are obtained.

$$u = \begin{cases} -i\{\delta_k \phi_{(k)} \sin\alpha_k + \sum_{i=1}^{2} \delta_l \phi_l^{(k)} \sin\alpha_l^{(k)} - \delta_3 \phi_3^{(k)} \cos\alpha_3^{(k)}\} k = 1, 2, \\ i\{\delta_k \phi_{(k)} \cos\alpha_k + \sum_{l=1}^{2} \delta_l \phi_l^{(k)} \sin\alpha_l^{(k)} - \delta_3 \varphi_3^{(k)} \cos\alpha_3^{(k)}\} k = 3, \end{cases}$$

$$w = \begin{cases} -i\{\delta_k \phi_{(k)} \cos\alpha_k + \sum_{i=1}^{2} \delta_l \phi_l^{(k)} \cos\alpha_l^{(k)} + (\phi_l^{(k)}/r) + \delta_3 \phi_3^{(k)} \sin\alpha_3^{(k)}\} k = 1, 2, \\ i\{\delta_k \phi_{(k)} \sin\alpha_k + \sum_{l=1}^{2} \delta_l \phi_l^{(k)} \cos\alpha_l^{(k)} + (\phi_l^{(k)}/r) + \delta_3 \varphi_3^{(k)} \sin\alpha_3^{(k)}\} k = 3. \end{cases} \tag{5}$$

Using these displacement components in Eq. (2), the nonzero stress components and fluid pressure are derived and are given by

$$\sigma_{rz} = \begin{cases} N\{\delta_k^2 \phi_{(k)} \sin 2\,\alpha_k - \sum_{l=1}^{2} \delta_l \phi_l^{(k)} \sin 2\,\alpha_l^{(k)} - (\phi_l^{(k)}/r^2) + \delta_3^2 \phi_3^{(k)} \cos\ 2\,\alpha_3^{(k)} + (i/r)\delta_l \phi_l^{(k)} \sin\alpha_l^{(k)}\}\ k = 1, 2, \\ N\{\delta_k^2 \phi_{(k)} \cos 2\,\alpha_k - \sum_{l=1}^{2} \delta_l \phi_l^{(k)} \sin 2\,\alpha_l^{(k)} - (\phi_l^{(k)}/r^2) + \delta_3^2 \phi_3^{(k)} \cos 2\,\alpha_3^{(k)} + (i/r)\delta_l \phi_l^{(k)} \sin\alpha_l^{(k)}\}\ k = 3, \end{cases}$$

$$\sigma_{zz} = \begin{cases} N\{-2\delta_k^2 \phi_{(k)} \cos^2\alpha_k + 2\sum_{l=1}^{2} \delta_i \phi_l^{(k)} \cos^2\alpha_l^{(k)} + N\delta_3^2 \phi_3^{(k)} \sin 2\alpha_3^{(k)}\} + (-i/r)\{(A + Q\mu_k)\delta_k \phi_{(k)} \sin\alpha_k \\ + \sum_{l=1}^{2} (A + Q\mu_l) \sin\alpha_l^{(k)} - (A + Q\mu_3)\delta_3 \phi_3^{(k)} \cos\alpha_3^{(k)} - N\delta_l \phi_l^{(k)} \cos\alpha_l^{(k)}\} \quad k = 1, 2, \\ N\{\delta_k^2 \phi_{(k)} \sin 2\alpha_k + \sum_{i=1}^{2} 2\delta_l^2 \phi_l^{(k)} \cos^2\alpha_l^{(k)} + N\delta_3^2 \phi_3^{(k)} \sin 2\alpha_3^{(k)} + (-i/r)\{(A + Q\mu_k)\delta_k \phi_{(k)} \cos\alpha_k \\ + \sum_{l=1}^{2} (A + Q\mu_l)\delta_l \phi_l^{(k)} \sin\alpha_l^{(k)} - (A + Q\mu_3)\delta_3 \phi_3^{(k)} \cos\alpha_3^{(k)} - N\delta_l \phi_l^{(k)} \cos\alpha_l^{(k)}\} \quad k = 3, \end{cases}$$

$$s = \begin{cases} \{(Q + R\mu_k)\delta_k^2 \phi_{(k)} \cos 2\alpha_k + \sum_{l=1}^{2} (Q + R\mu_l)\delta_l^2 \phi_l^{(k)} \cos 2\alpha_l^{(k)}\} + (-i/r)\{(Q + R\mu_k)\delta_k \phi_{(k)} \sin\alpha_k + \\ \sum_{l=1}^{2} (Q + R\mu_l)\delta_l \phi_l^{(k)} \sin\alpha_l^{(k)} - (Q + R\mu_3)\delta_3 \phi_3^{(k)} \sin\alpha_3^{(k)}\} k = 1, 2, \\ \{(Q + R\mu_k)\delta_k^2 \phi_{(k)} \sin 2\alpha_k + \sum_{i=1}^{2} (Q + R\mu_l)\delta_l^2 \phi_l^{(k)} \cos 2\alpha_l^{(k)}\} + (-i/r)\{(Q + R\mu_k)\delta_k \phi_{(k)} \cos\alpha_k + \\ \sum_{l=1}^{2} (Q + R\mu_l)\delta_l \phi_l^{(k)} \sin\alpha_l^{(k)} - (Q + R\mu_3)\delta_3 \phi_3^{(k)} \sin\alpha_3^{(k)}\} k = 3, \end{cases} \tag{6}$$

In Eq. (6), $\mu_l = \frac{(\rho_{11}R - \rho_{12}Q) - (PR - Q^2)V_l^{-2}}{(\rho_{22}Q - \rho_{12}R)}$, $\mu_k = \frac{(\rho_{11}R - \rho_{12}Q) - (PR - Q^2)V_k^{-2}}{(\rho_{22}Q - \rho_{12}R)}$, $k, l = 1, 2,\ 3$, where $V_1$ and $V_2$ are the velocities of dilatational waves of the first and second kind, respectively, and $V_3$ is the velocity of shear wave.

## 3 Boundary conditions

For permeable and stress-free base, the boundary conditions are given by

$$\sigma_{zz} + s = 0, \sigma_{rz} = 0, s = 0, \text{ at } z = 0. \tag{7}$$

From Eqs. (6) and (7), the following relations are obtained.

$$\sum_{l=1}^{3} A_{il}^{(k)} Z_l^{(k)} = A_{i\,0}^{(k)}, \quad k, l = 1, 2, 3, \tag{8}$$

where $A_{il}^{(k)}$ are

$$\begin{aligned} A_{1l}^{(k)} &= (2N\cos^2\alpha_k + ((A + Q) + (Q + R)\mu_l)\cos 2\alpha_k)\delta_k^2 - 2((A + Q) + (Q + R)\mu_l \\ &\quad (\sin\alpha_k - \cos\alpha_k)\delta_l),\ k = 1, 2, \\ A_{13}^{(k)} &= (N + ((A + Q) + (Q + R)\mu_l)\sin 2\alpha_k)\delta_3^2 - 2((A + Q) + (Q + R)\mu_l \cos\alpha_k)\delta_3), \\ A_{2l}^{(k)} &= (-(N\sin 2\alpha_k \delta_l^2 + N\sin\alpha_k \delta_l + N)), \quad k = 1, 2,\ A_{23}^{(k)} = N\cos 2\alpha_3 \delta_3^2, \end{aligned}$$

$$
\begin{aligned}
A_{3l}^{(k)} &= (Q+R\mu_l)\cos 2\alpha_k\delta_l^2 - 2(Q+R\mu_l)\sin\alpha_k\delta_l,\ k=1,2,\ A_{33}^{(k)} = -(Q+R\mu_3)\cos\alpha_3\delta_3,\\
A_{10}^{(k)} &= (-2N\cos^2\alpha_k + ((A+Q)+(Q+R)\mu_k)\cos 2\alpha_k)\delta_k^2\\
&\quad -2((A+Q)+(Q+R)\mu_k\sin\alpha_k\delta_k),\quad k=1,2,\\
A_{20}^{(k)} &= N\sin 2\alpha_k\delta_k^2,\ k=1,2,\ A_{20}^{(3)} = N\cos 2\alpha_k\delta_3^2,\\
A_{30}^{(k)} &= (Q+R\mu_k)\cos 2\alpha_k\delta_k^2 - (Q+R\mu_k)\sin\alpha_k\delta_k,\quad k=1,2,\\
A_{30}^{(3)} &= (Q+R\mu_3)\sin 2\alpha_3\delta_3^2 - (Q+R\mu_k)\cos\alpha_3\delta_3.
\end{aligned}
\tag{9}
$$

When a fast $P$-wave $(P-I)$ is incident, slow $P$-wave $(P-II)$ is incident and for a shear $SV$-wave, the reflection coefficients are

$$
Z_l^{(k)} = \frac{A_{10}^{(k)} + A_{20}^{(k)} + A_{30}^{(k)} - (A_{1l}^{(k)} + A_{2l}^{(k)} + A_{3l}^{(k)})(A_l^{(2)}/A_k) - (A_{1l}^{(k)} + A_{2l}^{(k)} + A_{3l}^{(k)})(A_l^{(3)}/A_k)}{(A_{1l}^{(k)} + A_{2l}^{(k)} + A_{3l}^{(k)})}, l,k = 1,2,3.
\tag{10}
$$

Similarly, the transmission coefficients are computed for body waves as that of reflection case. The expressions for transmission coefficients are similar as those of Eqs. (8)–(10), where Cos function is replaced by Sin function.

## 4 Numerical results

The reflection, transmission coefficients and energy ratio are computed for permeable base by introducing the non-dimensional parameters given by

$$
\begin{aligned}
&a_1 = \frac{P}{H}, a_2 = \frac{Q}{H}, a_3 = \frac{R}{H}, a_4 = \frac{N}{H}, d_1 = \frac{\rho_{11}}{\rho}, d_2 = \frac{\rho_{12}}{\rho}, d_3 = \frac{\rho_{22}}{\rho},\\
&H = P+2Q+R, \rho = \rho_{11}+2\rho_{12}+\rho_{22}.
\end{aligned}
\tag{11}
$$

The energy balanced equation is $E_1^{(k)} + E_2^{(k)} + E_3^{(k)} = 1,\quad (k=1,2,3)$, [13], where

$$
E_l^{(k)} = \left(\frac{\gamma_{11}+2\gamma_{12}\mu_l+\gamma_{22}\mu_l^2}{\gamma_{11}+2\gamma_{12}\mu_k+\gamma_{22}\mu_k^2}\right)\frac{\sqrt{\wedge_l/\wedge_k - \sin^2\alpha_k}}{\cos\alpha_k}(Z_l^{(k)})^2, k,l = 1,2,3.
\tag{12}
$$

Here $\mu_l = \frac{(a_3d_1-a_2d_2)-(a_1a_3-a_2^2)\wedge_l}{(a_2d_3-a_3d_2)}$, $\mu_k = \frac{(a_3d_1-a_2d_2)-(a_1a_3-a_2^2)\wedge_k}{(a_2d_3-a_3d_2)}$, $\Lambda_k = \left(\frac{V_0}{V_k}\right)^2$, $\Lambda_l = \left(\frac{V_0}{V_l}\right)^2$, $k,l = 1,2,\ 3,$ are the normalized phase velocities of $k$th incidented and $l$th reflected waves, respectively. In the above, $V_0 = \sqrt{\frac{H}{\rho}}$ is the reference velocity, $V_1$ and $V_2$ are the velocities of dilatational waves of the first and second kind, respectively, and $V_3$ is the velocity of shear wave. First reflection coefficient $Z_l^{(k)}$ is computed and hereby energy ratio is computed using Eq. (12) for permeable base. For illustration purpose, two types of poroelastic solid cylinders are used, namely cylinder-I made up of sandstone saturated with kerosene [22] and cylinder-II made up of sandstone saturated with water [23]. The physical parameter values and normalized phase velocities of these materials are given in Tables 1 and 2. Employing these values in Eq. (9), reflection, transmission coefficients and energy ratios are computed as a function of angle of incidence for a fixed wavenumber and the results are depicted in Figs. 2, 3, 4, 5, 6, 7, 8, 9, 10, 11, 12, 13, 14, 15, 16, 17, 18 and 19. The notations RCCyl-I, RCCyl-II, TCCyl-I, TCCyl-II, ERCyl-I and ERCyl-II used in the figures represent the reflection coefficient of cylinder-I, reflection coefficient of cylinder-II, transmission coefficient of cylinder-I, transmission coefficient of cylinder-II, energy ratio of cylinder-I and energy ratio of cylinder-II, respectively. The following particular cases are considered.

**Table 1** Material parameters

| Material parameters | $a_1$ | $a_2$ | $a_3$ | $a_4$ | $d_1$ | $d_2$ | $d_3$ |
|---|---|---|---|---|---|---|---|
| Cylinder-I | 0.843 | 0.065 | 0.027 | 0.234 | 0.901 | −0.001 | 0.1 |
| Cylinder-II | 0.96 | 0.006 | 0.029 | 0.412 | 0.876 | 0 | 0.124 |

**Table 2** Normalized phase velocities

| Material | $\frac{1}{\sqrt{\Lambda_1}}$ | $a_2$ | $\frac{1}{\sqrt{\Lambda_3}}$ |
|---|---|---|---|
| Cylinder-I | 1.0008427 | 0.4531887 | 0.5096217 |
| Cylinder-II | 1.047029 | 0.4832048 | 0.6857985 |

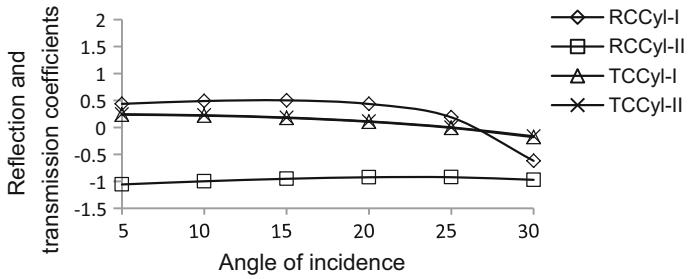


**Fig. 2** Reflection and transmission coefficients as a function of angle of incidence (in degrees) for $Z_1^{(1)}$

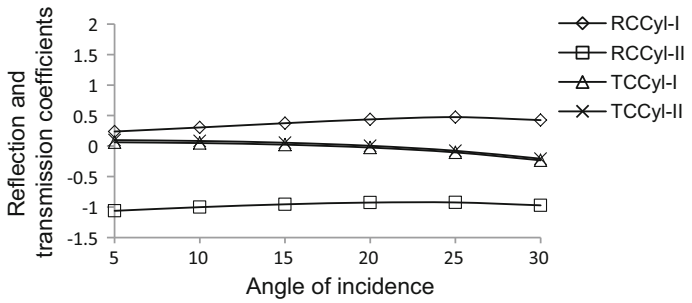


**Fig. 3** Reflection and transmission coefficients as a function of angle of incidence (in degrees) for $Z_2^{(1)}$

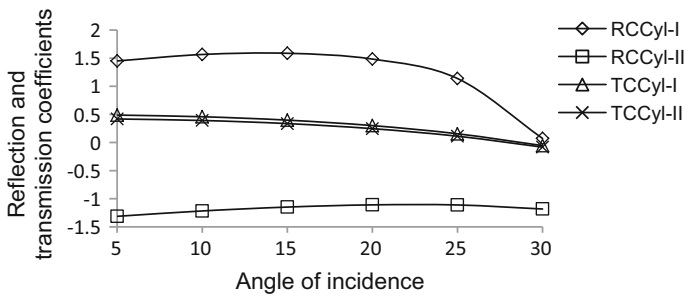


**Fig. 4** Reflection and transmission coefficients as a function of angle of incidence (in degrees) for $Z_3^{(1)}$

## 4.1 Incident fast dilatational wave

The reflection coefficient $Z_i^{(1)}(i = 1, 2, 3)$ and transmission coefficient $T_i^{(1)}(i = 1, 2, 3)$ are obtained as a function of angle of incidence in the case of $P - I$ wave, and the results are depicted in Figs. 2, 3 and 4. From these figures, it is seen that as angle of incidence increases, the reflection coefficient, in general, increases

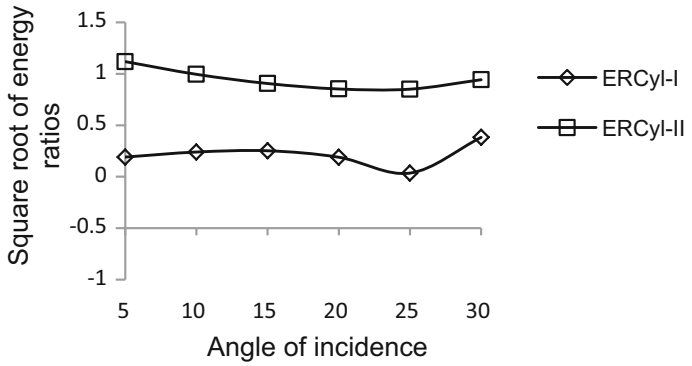


**Fig. 5** Energy ratios as a function of angle of incidence (in degrees) for $E_1^{(1)}$

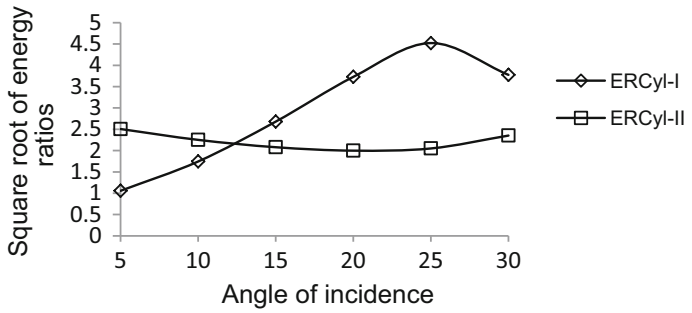


**Fig. 6** Energy ratios as a function of angle of incidence (in degrees) for $E_2^{(1)}$

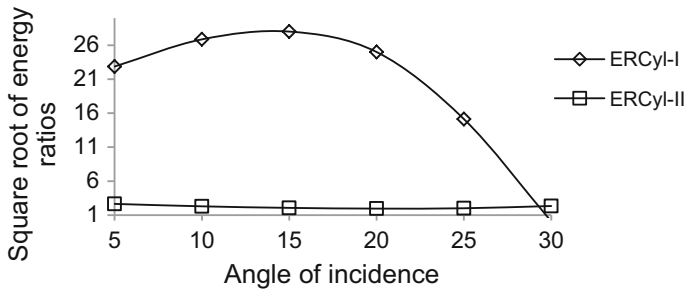


**Fig. 7** Energy ratios as a function of angle of incidence (in degrees) for $E_3^{(1)}$

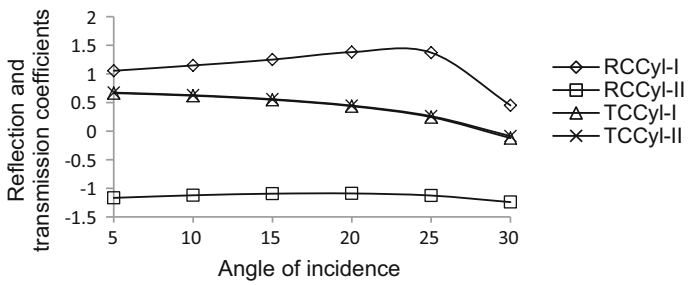


**Fig. 8** Reflection and transmission coefficients as a function of angle of incidence (in degrees) for $Z_1^{(2)}$

and transmission coefficient, in general, decreases for both the cylinders. In the case of cylinder-II, reflection coefficients $Z_1^{(1)}$, $Z_2^{(1)}$, $Z_3^{(1)}$ are negative. When the angle of incidence is 15°, reflection coefficient ($Z_1^{(1)}$) has maximum value. When the angle of incidence is 25°, transmission coefficient ($T_1^{(1)}$) has a minimum value. The

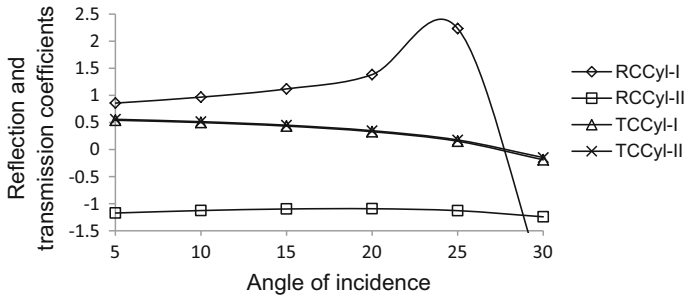


**Fig. 9** Reflection and transmission coefficients as a function of angle of incidence (in degrees) for $Z_2^{(2)}$

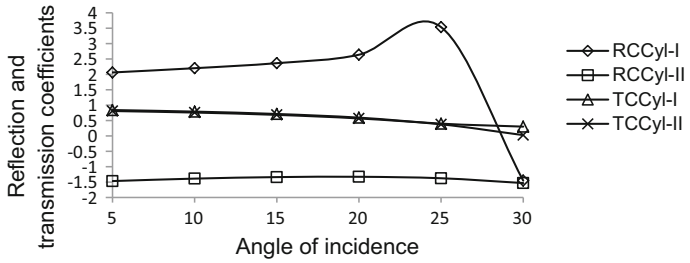


**Fig. 10** Reflection and transmission coefficients as a function of angle of incidence (in degrees) for $Z_3^{(2)}$

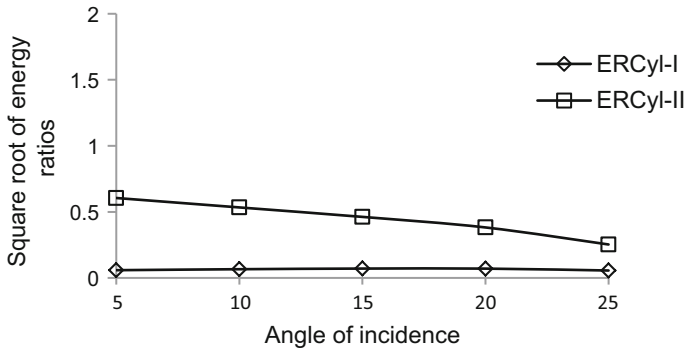


**Fig. 11** Energy ratios as a function of angle of incidence (in degrees) for $E_1^{(2)}$

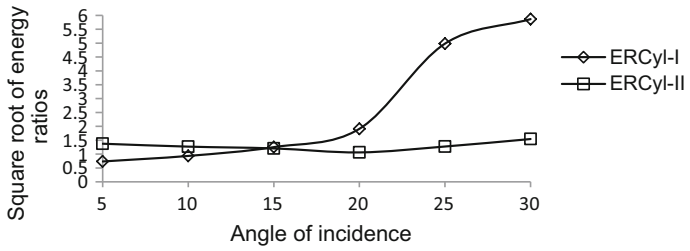


**Fig. 12** Energy ratios as a function of angle of incidence (in degrees) for $E_2^{(2)}$

energy ratio $E_i^{(1)}$ $(i = 1, 2, 3)$ for fast $(P - I)$ wave, slow $(P - II)$ wave and shear $(SV)$ wave is computed as a function of angle of incidence, and the results are depicted in Figs. 5, 6 and 7. In Fig. 5, it is seen that the energy ratios for cylinder-I are, in general, lower than that of cylinder-II. From Figs. 6 and 7, it is clear that the energy ratios for cylinder-I are, in general, higher than that of cylinder-II. From Fig. 7, it is clear that energy ratios $(E_3^{(1)})$ are very high in the case of reflected shear wave.

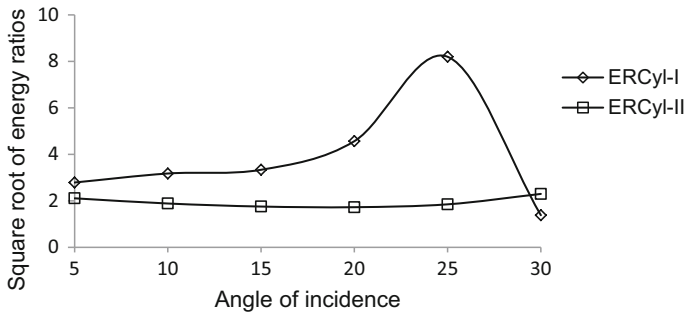


**Fig. 13** Energy ratios as a function of angle of incidence (in degrees) for $E_3^{(2)}$

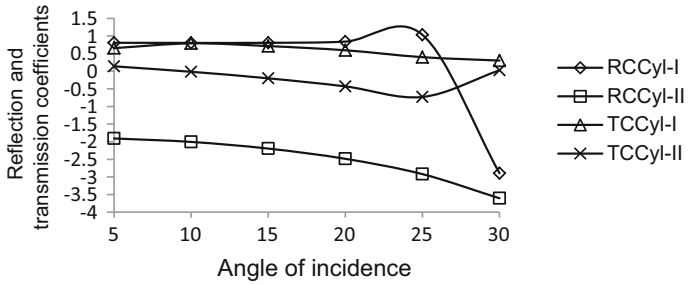


**Fig. 14** Reflection and transmission coefficients as a function of angle of incidence (in degrees) for $Z_1^{(3)}$

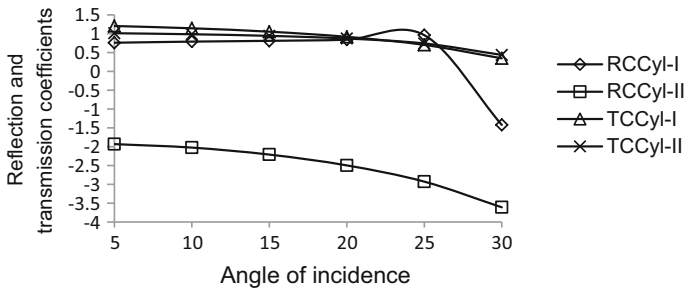


**Fig. 15** Reflection and transmission coefficients as a function of angle of incidence (in degrees) for $Z_2^{(3)}$

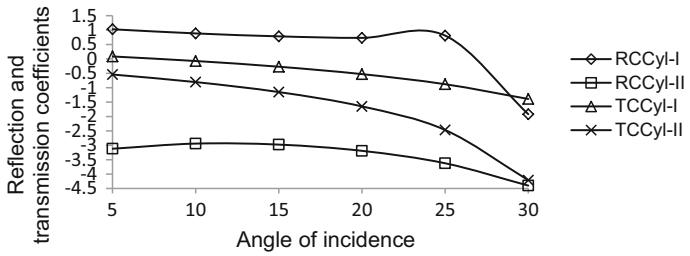


**Fig. 16** Reflection and transmission coefficients as a function of angle of incidence (in degrees) for $Z_3^{(3)}$

## 4.2 Incident slow dilatational wave

The reflection coefficients $Z_i^{(2)}(i = 1, 2, 3)$ and transmission coefficients $T_i^{(2)}$ $(i = 1, 2, 3)$ are obtained as a function of angle of incidence in the case of slow $P - II$ wave. The pertinent results are depicted in Figs. 8, 9 and 10. From these figures, it is seen that as angle of incidence increases, the reflection coefficient, in general, increases, but the transmission coefficient, in general, decreases. The reflection coefficients $Z_1^{(2)}$, $Z_2^{(2)}$, $Z_3^{(2)}$

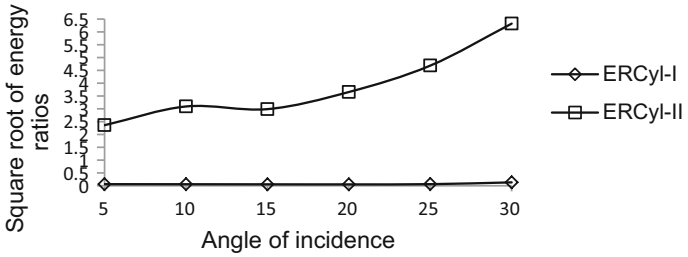


**Fig. 17** Energy ratios as a function of angle of incidence (in degrees) for $E_1^{(3)}$

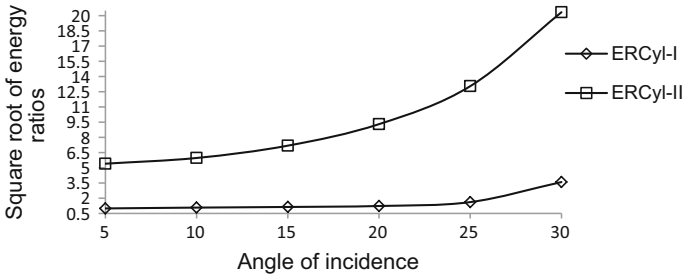


**Fig. 18** Energy ratios as a function of angle of incidence (in degrees) for $E_2^{(3)}$

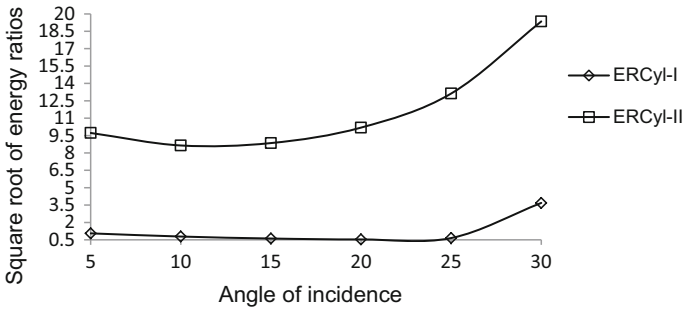


**Fig. 19** Energy ratios as a function of angle of incidence (in degrees) for $E_3^{(3)}$

are negative for cylinder-II. When angle of incidence is 25°, the reflection coefficient has maximum value and has minimum value when the incident angle is 30°. The energy ratios are computed against angle of incidence, and the results are depicted in Figs. 11, 12 and 13. From these figures, it is clear that $E_1^{(2)}$ gradually increases. Also, it is clear that energy ratios for cylinder-I are, in general, higher than that of the cylinder-II. From Fig. 13, it is observed that energy ratios ($E_3^{(2)}$) are very high in the case of reflected shear wave. When the angle of incidence is 15°, energy ratios ($E_2^{(2)}$) of both the cylinders coincide in the case of reflected shear wave.

### 4.3 Shear incident wave

The reflection coefficients $Z_i^{(3)}$ $(i = 1, 2, 3)$ and transmission coefficients $T_i^{(3)}$ $(i = 1, 2, 3)$ are computed as a function of angle of incidence in the case of shear $SV$ wave. The relevant results are depicted in Figs. 14, 15 and 16. From these figures, it is clear that the reflection coefficient, in general, increases in the case of cylinder-I, and the result is reversed in the case of cylinder-II, whereas the transmission coefficient, in general, decreases for both the cylinders. When the angle of incidence is 30°, the reflection coefficient of cylinder-II has minimum value. Energy ratios $E_1^{(3)}$, $E_2^{(3)}$, $E_3^{(3)}$ are computed for fast $(P-I)$ wave, slow $(P-II)$ wave and shear $(SV)$ wave, and the results are depicted in Figs. 17, 18 and 19. From these figures, it is observed that energy ratios of cylinder-II are higher than that of cylinder-I. From Fig. 17, it is observed that energy ratios of cylinder-I are slightly linear in nature.

## 5 Conclusion

Employing the Biot's poroelasticity theory, two wave phenomena, namely reflection and transmission, are investigated. The energy ratios are computed for two dilatational waves and one shear wave in the case of permeable base. For numerical process, two types of solids , namely sandstone saturated with kerosene (say cylinder-I) and sandstone saturated with water (say cylinder-II), are employed, and the results are presented graphically. From the numerical results, it is observed that in the case of cylinder-I, reflection coefficient for fast and slow dilatational waves increases and, for shear wave, it decreases. In the case of cylinder-II, the results are reversed. Both the materials are sandstone related and differ only in the fluid part. Thus, it can be inferred that the fluid part causes the above discrepancy. For all the waves, reflection and transmission coefficients for cylinder-II are negative. The energy ratios increase for all the waves, in the case of both cylinder-I and cylinder-II.

**Acknowledgements** Authors acknowledge Department of Science and Technology (DST) for funding through Fund for Improvement of S&T Infrastructure (FIST) program sanctioned to the Department of Mathematics, Kakatiya University, Warangal, with File No. SR/FST/MSI-101/2014. One of the authors Rajitha Gurijala acknowledges University Grants Commission (UGC), Government of India, for its financial support through the Postdoctoral Fellowship for Women (Grant No. F.15-1/2015-17/PDFWM-2015-17-TEL-34525 (SA-II)).

## References

1. Schoenberg, M.: Elastic wave behavior across linear slip interfaces. J. Acoust. Soc. Am. **68**, 1516–1521 (1980)
2. Bogy, D.B., Gracewski, S.M.: Reflection coefficient for plane waves in a fluid incident on a layered elastic half -space. J. Appl. Mech. **50**(2), 405–414 (1983)
3. Singh, B.: Reflection of P and SV waves from the free surface of an elastic solid with generalized thermo diffusion. J. Earth Syst. Sci. **114**, 159–168 (2005)
4. Kumar, R., Kansal, T.: Reflection and refraction of plane waves at the interface of an elastic solid half space and a thermo elastic diffusive solid half space. Arch. Mech. **64**, 293–317 (2012)
5. Kumar, R., Sanjeev, A., Garg, S.K.: Reflection and transmission of plane waves at the loosely bounded interface of an elastic solid half space and a micro stretch thermo elastic diffusion solid half space. Mater. Phys. Mech. **21**, 147–167 (2014)
6. Sharma, J.N., Kaur, R.: Study of reflection and transmission of plane waves at thermo elastic diffusive solids/liquid interface. Latin Am. J. Solids Struct. **11**, 2141–2170 (2014)
7. Wu, K.Y., Xue, Q., Adler, L.: Reflection and transmission of elastic waves from a fluid saturated porous solid boundary. J. Acoust. Soc. Am. **87**, 2349–2358 (1990)
8. Santos, J.E., Corbero, J.M., Ravazzoli, C.L., Hensley, J.L.: Reflection and transmission coefficients in fluid-saturated porous media. J. Acoust. Soc. Am. **91**, 1911–1923 (1992)
9. Badiey, M., Jaya, I., Cheng, A.: Plane wave reflection from anisotropic poroelastic sediment overlying isotropic poroelastic half space. J. Comput. Acoust. **99**(2), 903–913 (1994)
10. Abd-Alla, A.N., Al-Dawy, A.S.: Reflection phenomena of SV-waves in generalized thermo elastic medium. Int. J. Math. Math. Sci. **23**, 529–546 (2000)
11. Lin, Q.R., Chen, Y.C., Trifunac, V., Michailo, : Reflection of plane waves in a poroelastic half-space saturated with non-viscous fluid. Solid Dyn. Earthq. Eng. **25**, 205–223 (2001)
12. Biot, M.A.: Theory of elastic wave in a fluid-saturated porous solid-I. J. Acoust. Soc. Am. **28**, 168–178 (1956)
13. Tajuddin, M., Hussaini, S.J.: Reflection of plane waves at boundaries of a liquid filled poroelastic half space. J. Appl. Geophys. **58**, 59–86 (2006)
14. Dai, Z.J., Kuang, Z.B.: Reflection and transmission of elastic waves at the interface between water and a double porosity solid. Transp. Porous Media **72**, 369–392 (2008)
15. Madeo, A., Gavrilyuk, S.: Propagation of acoustic waves in porous media and their reflection and transmission at a pure fluid/porous medium permeable interface. Eur. J. Mech./A Solids **29**, 897–920 (2010)
16. Cui, Z.W., Wang, K.X.: Influence of the squirt flow on reflection of elastic waves at a fluid saturated poroelastic solid interface. Int. J. Eng. Sci. **41**, 2179–2191 (2003)
17. Ethyl, K., Duwadare, Q.J., Oyewumi, K.J.: Semi relativistic reflection and transmission coefficients for two spinless particles. Commun. Theory Phys. **66**, 389–395 (2016)
18. Kumar, R., Miglani, A., Kumar, S.: Reflection and transmission of plane waves between two different fluids saturated porous half spaces. Bull. Pol. Acad. Sci. Tech. Sci. **59**(2), 227–234 (2011)
19. Corredor, R.M., Santos, J.E., Gauzellino, P.M., Carcione, J.M.: Reflection and transmission coefficients of single layer in poroelastic media. J. Acoust. Soc. Am. **135**(6), 3151–3162 (2014)
20. Malla Reddy, P., Tajuddin, M.: Exact analysis of the plane strain vibrations of thick walled hollow poroelastic cylinders. Int. J. Solids Struct. **37**, 3439–3456 (2000)
21. Zine, A.F., Mohamed, F., Depollier, C., Ogam, E., Mitri, F.G.: Wave propagation in porous materials. In: Reyhanoglu, M. (ed.) Computational and Experimental Studies of Acoustic Waves, 1st edn. InTech, London (2018). https://doi.org/10.5772/65135
22. Yew, C.H., Jogi, P.N.: Study of wave motions in fluid-saturated porous rocks. J. Acoust. Soc. Am. **60**, 2–8 (1976)
23. Fatt, I.: The Biot–Willis elastic coefficient for a sand stone. J. Appl. Mech. **26**, 296–297 (1957)